

Generalized half-center oscillators with short-term synaptic plasticity

V. Baruzzi,¹ M. Lodi,¹ M. Storace,¹ and A. Shilnikov²

¹*Department of Electrical, Electronics and
Telecommunication Engineering and Naval Architecture,
University of Genoa, 16145 Genoa, Italy*

²*Department of Mathematics and Statistics,
Neuroscience Institute, Georgia State University, Atlanta, GA 30303 USA.*

(Dated: May 22, 2020)

Abstract

How can we develop simple yet realistic models of the small neural circuits known as central pattern generators (CPGs), which contribute to generate complex multi-phase locomotion in living animals? In this paper we introduce a new model (with design criteria) of a generalized half-center oscillator (gHCO), (pools of) neurons reciprocally coupled by fast/slow inhibitory and excitatory synapses, to produce either alternating bursting or synchronous patterns depending on the sensory or other external input. We also show how to calibrate its parameters, based on both physiological and functional criteria and on bifurcation analysis. This model accounts for short-term neuromodulation in a bio-physically plausible way and is a building block to develop more realistic and functionally accurate CPG models. Examples and counterexamples are used to point out the generality and effectiveness of our design approach.

I. INTRODUCTION

Central pattern generators (CPGs) are small neural circuits that can autonomously (i.e., in the absence of sensory feedback or higher motor planning centers inputs) produce various rhythmic patterns of neural activity [17]. They bear a fundamental function in both invertebrate and vertebrate animals as they determine multi-phase locomotion – the innate motor behavior that requires sequential activation of body muscles in a coordinated way [22]. Various approaches to the modeling of CPGs and CPG-inspired control systems have been explored in the last decades [7, 12, 18, 30, 37]. Recently, new methods have been proposed to reduce large models of detailed neural networks to smaller CPG circuits, trading off biological plausibility and complexity of the model [2, 7, 25, 27, 30].

Although CPGs function autonomously, their activity is modulated through the influence of hierarchically higher areas, which can, for example, prompt transitions between gaits [9, 15, 34]. A single gait in a typical CPG model is obtained by fixing the connectivity. By contrast, to generate multiple gaits the CPG connections between constituent neurons are typically changed acting on the synaptic weights to model the control action of the brainstem [12, 25–27]. The modulation from higher areas that controls the synchronization between the CPG neurons, and thus triggers gait switches, is conveniently integrated in CPG models to directly affect the synaptic conductance strengths. However, in real CPGs changes in conductance values are the result of long-term synaptic plasticity, and therefore it is hardly a cause for quick gait switches, which can instead be accounted for more realistically by short-term neuromodulation. Indeed, most natural CPGs exhibit patterns of functional connectivity between neurons or synchronized clusters of neurons that can undergo spontaneous fluctuations and be highly responsive to perturbations, e.g., induced by sensory input or cognitive tasks, on a timescale of milliseconds or hundreds of milliseconds, respectively, thus ensuring robustness and stability. This short-term neuromodulation lacks in most CPG models.

One of the pivotal building blocks of many CPGs is a half-center oscillator (HCO). The HCO-concept is widely used to model two synchronous pools of neurons reciprocally inhibiting each other to produce stable rhythmic alternation in animal locomotion [6, 10]. This basic structure has been largely studied from both biological and nonlinear dynamics standpoints. For example, in [4] transitions between stable synchronous states in the HCO

occur through direct manipulations with synaptic weights, whereas in [14] a large database of HCO models is swept using a brute-force approach, without a focus on gait transitions. While the importance of an interplay between inhibitory and excitatory coupling has already been outlined [4], the thorough understanding of its functional role for determining multiple states or patterns in such neural networks and how transitions between them may stably occur remains yet insufficient. Moreover, there is the growing evidence that (i) post-synaptic potential (PSP) summation increasing with the spike frequency in the pre-synaptic cell is a crucial factor for stable functioning of some CPGs [11, 16, 29, 32], while other experiments indicate that (ii) the activity of some synapses is barely affected by the spike frequency [12]. In this paper, we propose a generalized half-center oscillator (gHCO) composed of two neurons or of two neural pools that are coupled reciprocally by excitatory synapses, in addition to the standard HCO's reciprocally inhibitory synapses. We show that this circuitry warrants a more biologically plausible mechanism of short-term plasticity to implicitly control the phase-lag between the gHCO cells by varying their spike frequency through sensory drive or external currents, rather than directly manipulating the synaptic conductance strengths. Moreover, we show how to calibrate the gHCO parameters in order to obtain the desired behaviors, also carrying out a numerical bifurcation analysis.

II. THE GHCO AND ITS DESIGN CONSTRAINTS

The proposed generalized half-center oscillator is shown in Fig. 1. It is made of two neurons or two neural pools, coupled by both excitatory (marked by a black circle) and inhibitory (marked by a black triangle) synapses.

There are a few simple constraints that neurons and synapses must meet for the circuit to generate stably the desired rhythmic outcomes: (a) both neurons are endogenous bursters with (b) the spiking voltage range above the hyperpolarized voltage (i.e., they do not *undershoot* [19]) within each burst, while (c) the mean spike frequency can be controlled. The gHCO bursters are coupled by (d) slow synapses with PSP summation whose strength increases with the growing spike frequency in presynaptic cells, as well as by (e) fast synapses without PSP summation.

In what follows, both gHCO cells are represented by the Hodgkin-Huxley (HH) type model of the thalamic reticular neuron [13, 28] (see Appendix). This slow-fast model with seven

state variables can exhibit endogenous bursting activity of alternating trains of fast action potentials with long quiescent intervals, as depicted in Fig. 2. The dynamics of the membrane potential V_j and of the voltage-dependent state variables (the vector \mathbf{y}_j) are governed by a generic set of HH-like equations

$$\frac{d}{dt} \begin{bmatrix} V_j \\ \mathbf{y}_j \end{bmatrix} = \begin{bmatrix} -\sum_k I_k + I_j^{syn} \\ f(V_j, \mathbf{y}_j) \end{bmatrix}, \quad \text{where } j = 1, 2. \quad (1)$$

where $f(V_j, \mathbf{y}_j)$ is a vector function describing \mathbf{y}_j -dynamics; in particular, each f component for the HH gating variables is a logistic function. In addition to intracellular currents, $\sum_k I_k$ includes a further external contribution, namely a control current I_c acting essentially on the spike frequency within bursts. For the given model, bursting activity occurs when $I_c \in [-0.43, 0.13] \left[\frac{\mu A}{cm^2} \right]$, with the mean spike frequency decreasing from 15.36 to 4.13 ms. The term I_j^{syn} is the incoming mixed, excitatory/inhibitory synaptic current originating from the i -th cell onto the j -th, post-synaptic cell:

$$I_j^{syn} = g^{ex}(E^{ex} - V_j)s_i^{ex} + g^{in}(E^{in} - V_j)s_i^{in}, \quad (2)$$

where $E^{ex/in}$ are the reversal potentials for excitatory/inhibitory synapses and $0 \leq s_i^{ex/in} \leq 1$ is the activation or neurotransmitter release rate of the synapse, excitatory ($V_j < E^{ex}$) or inhibitory ($V_j > E^{in}$). For the slow synapses with PSP summation we employ a first-order dynamic synapse [8, 21, 35]. The dynamic evolution of its activation rate is governed by the following equation

$$\frac{ds_i}{dt} = \alpha(1 - s_i)f_\infty(V_i) - \beta s_i, \quad f_\infty = \frac{1}{1 + e^{-\nu(V_i - \theta)}}, \quad (3)$$

where θ is the synaptic threshold, whereas α and β are coefficients weighting the raise and decay terms, respectively. To model the static synapses without PSP summation we employ

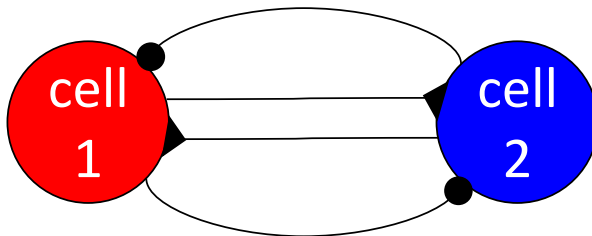


FIG. 1. (color online). gHCO neural circuit with inhibitory (denoted with $\blacktriangleright \blacktriangleleft$) and excitatory (\bullet) synapses reciprocally coupling two oscillatory cells.

the fast threshold modulation paradigm [33] using the sigmoidal function: $0 \leq s_i = f_\infty(V_i) \leq 1$, with θ being below the spike-level.

To illustrate the contrasting properties of these synapse models, we refer to Fig. 2, showing the bursting voltage traces V_1 (red) and V_2 (blue) and the synaptic activation dynamics, fast $s_2^{in}(t)$ (gray) and slow $s_2^{ex}(t)$ (black) at the edge of the I_c bursting interval. Observe that the neurotransmitter release rate $s_2^{in}(t)$ of the fast FTM synapse (1) is maximized as soon as the voltage $V_2(t)$ in the pre-synaptic cell overcomes the synaptic threshold θ^{in} (indicated by the grey lines in panels a,b), (2) remains constant regardless of the spike frequency, and (3) vanishes with the burst termination. In contrast, the low spike frequency (panels a,c) barely activates the slow synapse (see $s_2^{ex}(t)$) that at high spike frequency (panels b,d) exhibits the profound PSP build up; the ascending rate is ruled by $\alpha > 0$, and the exponential decay due to $\beta > 0$ starts after the voltage lowers below θ .

III. PARAMETER CALIBRATION

The neuron and synapse models (1-3) are calibrated to physiologically plausible values to meet the above requirements (a)-(e) and to ensure a smooth and reversible transition from anti-phase to in-phase bursting occurring in the gHCO as the spike frequency changes due to I_c -variations. Just to clarify things, let us consider the dynamics of the gHCO with fast FTM inhibitory and slow excitatory synapses. Moreover, the corresponding synaptic thresholds are set at $\theta^{in} = -30$ and $\theta^{ex} = 25\text{mV}$, respectively. As such, the inhibitory synapses without PSP summation (de)-activate quickly and their strength remain constant during each burst regardless of the spike frequency. In contrast, the slow excitatory synapses exhibit PSP summation that becomes stronger with an increase of the spike frequency.

Figure 2 shows that at the low end $I_c = -0.43$ of the bursting region, near the transition to the hyperpolarized quiescence, the gHCO neurons oscillate in anti-phase with the smallest number of spikes per burst and lowest spike frequency (panels (a, c)), whereas on the opposite side at $I_c = 0.13$ the neurons burst in phase with a larger number of spikes per burst and with much higher spike frequency (panels (b, d)). Changing the value of I_c changes the strength of the excitatory synapses, and hence the proportion between inhibition and excitation that repel the gHCO neurons or attract them to each other, respectively. The *phase-lag* Δ (defined on mod 1) between burst initiations in the neurons [20, 36, 38] allows

quantifying the phase-locked states produced by the gHCO. In case of the synchronous or in-phase bursters, $\Delta = 0$ (or $\Delta = 1$). When they burst in alternation, with $\Delta = 0.5$, we say that they are in anti-phase. The intermediate values of Δ correspond to “winner-less” patterns transitional between the in- and anti-phase states generated by the gHCO.

The bifurcation analysis of the system (1–3) was carried out using the computational toolbox CEPAGE [24]. Since we want the gHCO to transition from anti-phase regime to in-phase regime varying I_c , we need the proportion between inhibition and excitation to be significantly different for the two values of I_c at the edges of its range. To this end, we seek maximum difference in the mean values of s_i^{ex} (over one period) at the two extreme values of I_c , i.e., -0.43 (anti-phase pattern) and 0.13 (in-phase bursting). We set the numerical values of θ^{ex} , α and β according to this principle, running a set of simulations over a

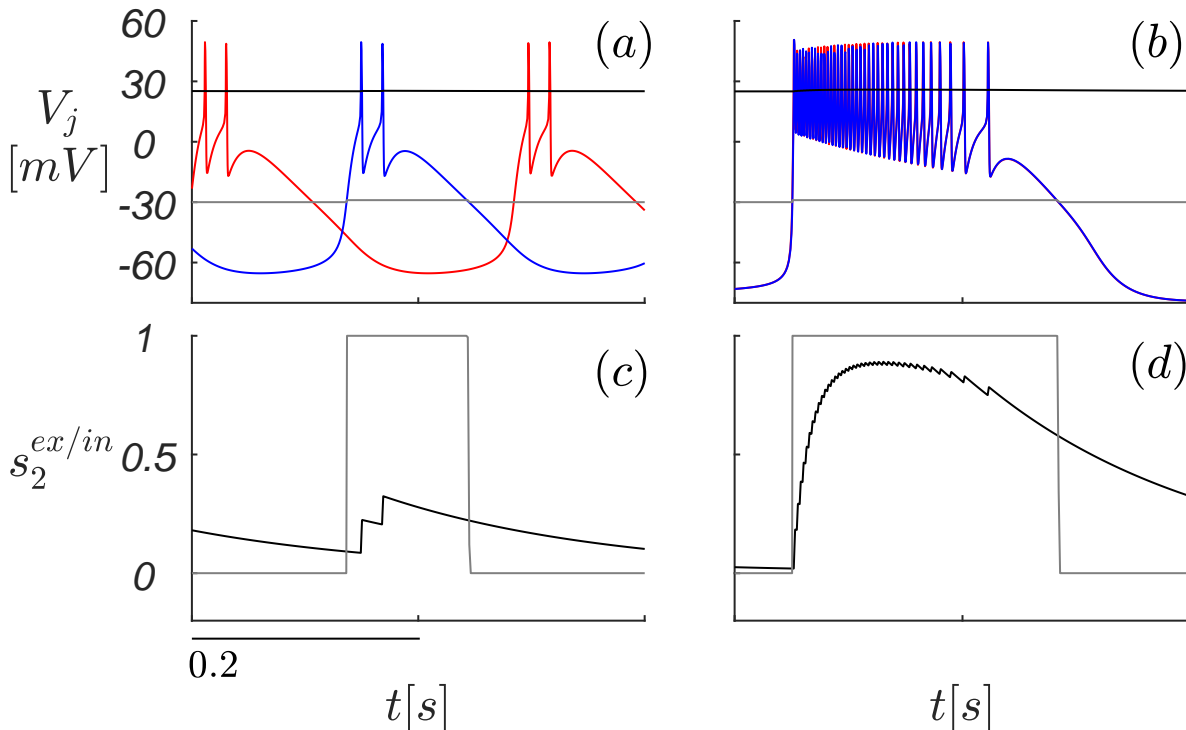


FIG. 2. (color online) Asymptotic anti-phase (a) and synchronous (b) bursting voltage traces V_1 (red) and V_2 (blue) at $I_c = -0.43$ and 0.13 , resp., in gHCO (1)-(3), superimposed with excitatory/inhibitory thresholds θ (horizontal lines) at 10 and -30 mV. (c,d) Synapse dynamics: fast modulatory $s_2^{in}(t)$ (gray) vs. slowly summing/decaying $s_2^{ex}(t)$ (black). See the Appendix for parameters.

grid of parameter values: $\theta^{ex} = \{10, 25\}$, 10 evenly spaced values of $\alpha \in [0.05, 1]$ and 10 evenly spaced values of $\beta \in [0.005, 0.1]$. The considered values of θ^{ex} indicate voltage levels representative of two different conditions: at $\theta^{ex} = 10$ each spike appears broader, i.e. V_j stays above θ^{ex} for a longer time window; at $\theta^{ex} = 25$ each spike appears narrower, i.e. V_j stays above θ^{ex} for a shorter time period. We choose the parameter setting that provides maximum difference in the mean values of s_i^{ex} for the two extreme values of I_c (see Appendix B). The synaptic conductances $g^{in/ex}$ are set to obtain anti-phase synchronization for low spike frequency, condition in which the mean value of s_i^{ex} is minimum, and in-phase synchronization for high spike frequency, condition in which the mean value of s_i^{ex} is maximum.

The results are summarized in Fig. 3, and reveal the dependence of the phase-lag Δ on the I_c -current, and hence explicitly on the spike frequency within bursts. As expected, at low I_c -values between -0.43 and -0.40 , the fast reciprocal inhibition within the gHCO dominates and makes its neurons burst in alternation with $\Delta = 0.5$. As the I_c -current is increased, the spike frequency raises, which in turn makes the slow excitatory synapses sum up faster and stronger on average. With larger I_c values, the reciprocal excitation gradually prevails over the reciprocal inhibition, which gives rise to the smooth onset of the

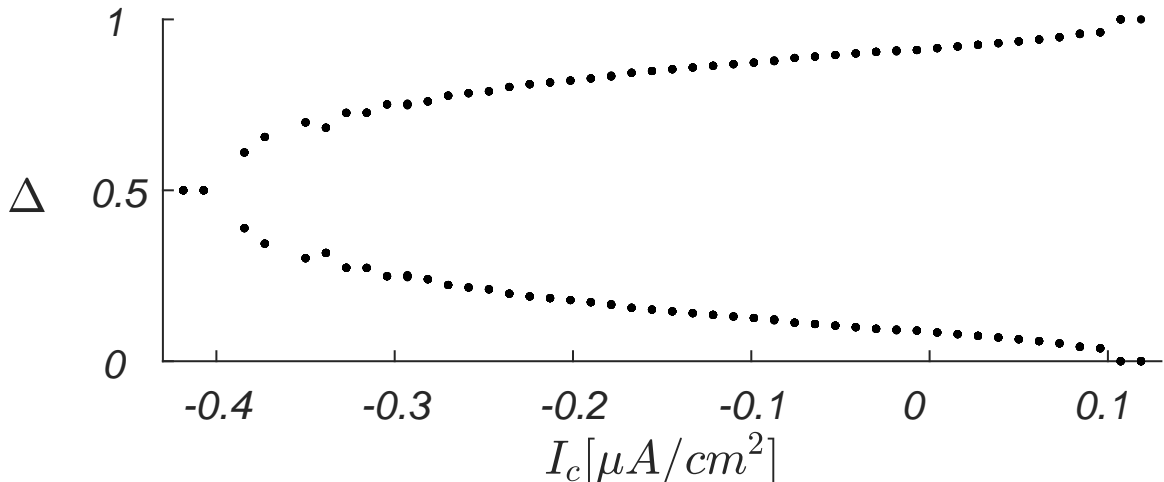


FIG. 3. Bifurcation diagram showing how the phase-lag Δ between the gHCO neurons is affected by the current I_c ; here, 30 initial Δ -values were sampled evenly between 0.05 and 0.95 for each of the 50 I_c -values. Parameters listed in the Appendix.

stable in-phase bursting in the gHCO. This is revealed in the bifurcation diagram with a characteristic pitchfork shape of the dependence of the phase-lag Δ on the I_c -current. We note also that this diagram has been obtained by making a multi-shooting for each parameter value. This is a direct indication that there is no hysteresis and therefore the absence of multi-stability or the coexistence of anti- and in-phase bursting for same parameter values, and that the transition between activity rhythms is continuous and reversible. We would like to re-emphasize that the maximal synaptic conductances $g^{in/ex}$ in Eq. (2) once set are not changed, and the transition is solely determined by the gradual increase/decrease of the mean s_i^{ex} -value caused by the spike frequency variations in the gHCO neurons.

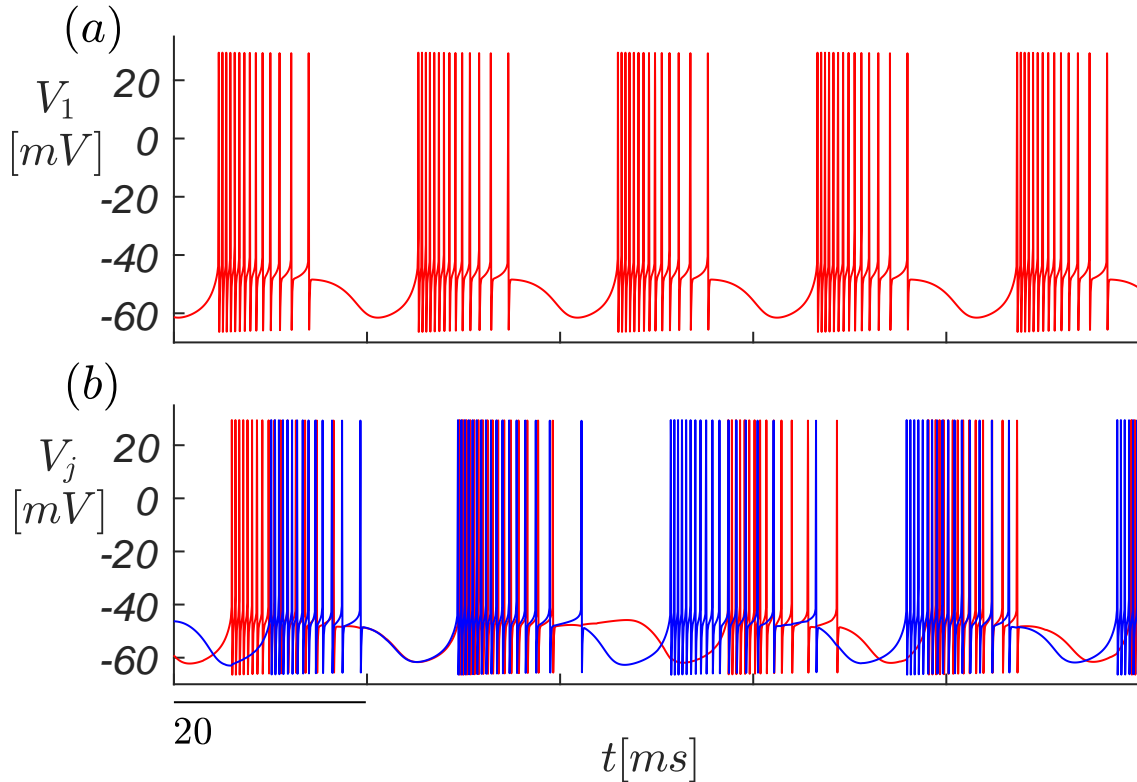


FIG. 4. (color online). (a) Asymptotic bursting voltage trace with undershoot produced by the Plant neuron model [1, 31]. (b) Voltage traces produced by the gHCO with two coupled Plant neurons. See the Appendix for parameters.

IV. COUNTEREXAMPLES

The proposed gHCO concept can fall apart whenever one or more of the conditions on the neuron and synapse models are not fulfilled. If the bursting condition (a) is broken, the approach is no longer applicable. Two neurons, spiking in isolation, can burst in alternation due to reciprocal inhibition, but not through reciprocal excitation, which makes both even more synchronously depolarized with a higher frequency. If the neurons under-shoot (condition (b)), which is typical for elliptical bursters [1] (see Fig. 4(a)), the choice of the inhibitory threshold θ^{in} to warrant evenly constant activation s_i^{in} requires additional considerations. Indeed, this choice can result in less robust dynamics of the gHCO, due to inhibition-excitation competition (see Fig. 4(b)). Condition (c), outlining the importance of being able to control spike-frequency and not only burst duration of the pre-synaptic cell, is quite crucial for stable gHCO functions. To point out its significance, we employ the exponential integrate-and-fire (eIF) neuron model [5], where an external current I_{ext} primarily controls the burst duration with insignificant spike-frequency variations, as shown in Fig. 5(a). In this scenario, the activation of both inhibitory and excitatory synapses is mainly determined by the burst duration in the eIF-neurons, and thus I_{ext} -variations can only cause proportional changes in the average excitatory s_i^{ex} - and inhibitory s_i^{in} -values. As a result, neither inhibition nor excitation can solely dominate and produce the expected solo stable anti-phase or in-phase bursting patterns within the given I_{ext} -range, as shown in Fig.5(b). Conversely, changing the parameter g_e of the eIF neuron model significantly modifies the spike frequency, and the corresponding bifurcation diagram has the characteristic pitchfork shape, as expected. However, the parameter g_e is a conductance, and thus is not a realistic control parameter, according to our guidelines. Condition (d) follows (c), as the synaptic threshold θ , for the slow synapses, has to be within the spike voltage range of the pre-synaptic neuron and the dynamics is to be slow enough to allow $s_i(t)$ to grow and the synapse to exhibit PSP summation. Condition (e) guarantees that the activation of the fast synapse does not exhibit PSP summation and hence does not change due to spike frequency variations in the pre-synaptic neuron.

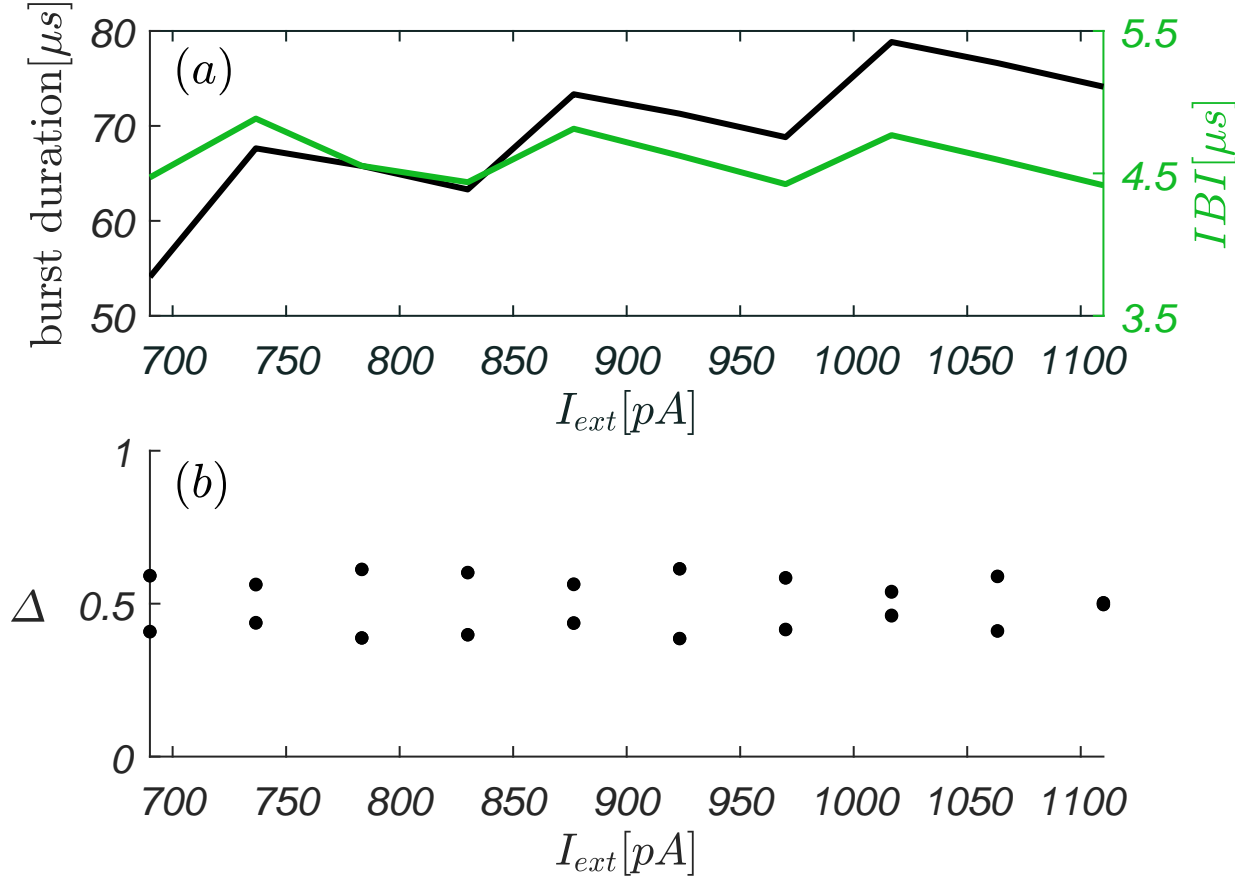


FIG. 5. (color online). (a) Mean values (over 5 s) of the IBI (green line) and the burst duration (black line) plotted against I_{ext} for the exponential IF-model [5]. Corresponding bifurcation diagram for the phase lag Δ between the cells in the gHCO, in which each cell is an exponential IF-model (b).

V. TOWARDS A LOCOMOTION CPG

As the gHCO often happens to be a CPG building block, we discuss some solutions ensuring that both the phase lags and the burst frequency are consistent for the modeled gaits. For instance, in left-right alternation of the mouse locomotion, a phase lag $\Delta = 0.5$ occurs at low burst frequencies (walk and trot gaits), whereas a phase lag Δ close to 0 (or to 1, equivalently) occurs at high burst frequencies (gallop and bound gaits) [3, 23, 26]. Recall that the thalamic reticular neuron model in isolation exhibits high frequency bursting at small I_c -values and slow bursting at greater I_c -values. Therefore, for the gHCO built with such models to produce in-phase/anti-phase synchronization at high/low burst frequencies

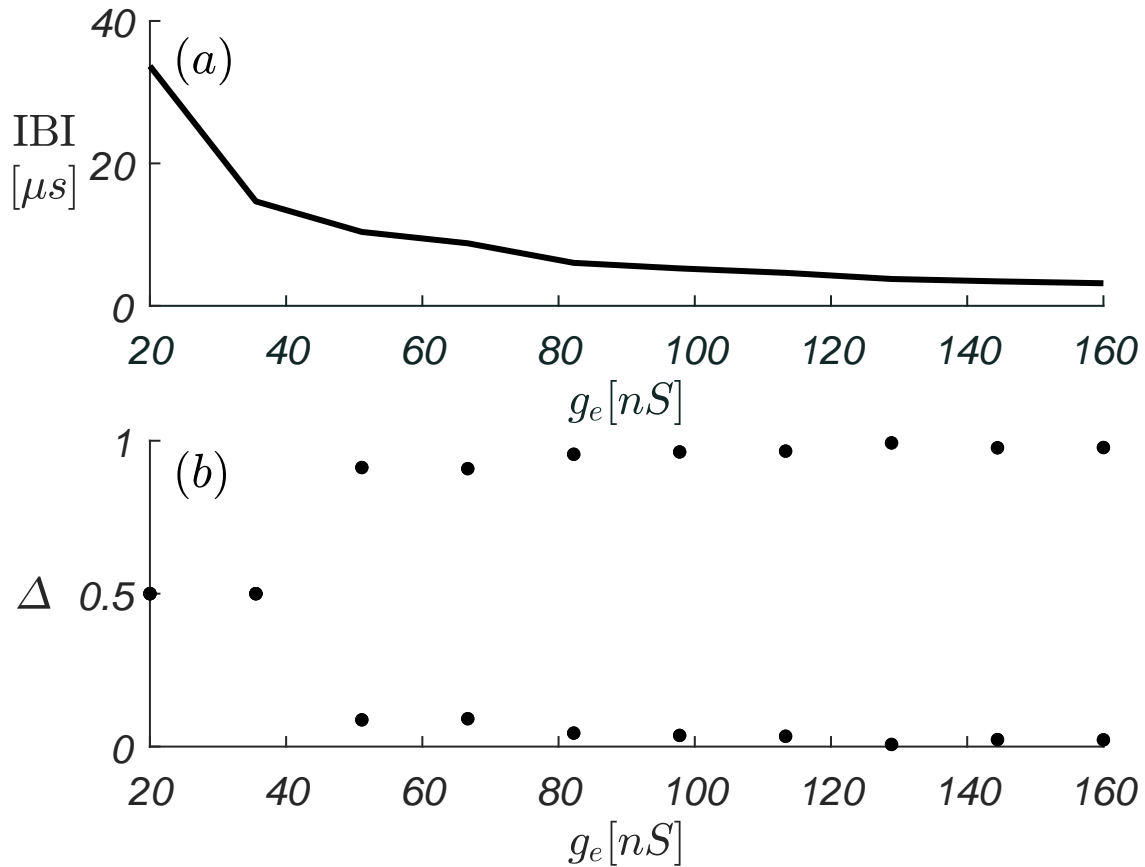


FIG. 6. (a) Mean values (over 5 s) of the IBI plotted against g_e for the exponential IF-model [5]. Corresponding bifurcation diagram for the phase lag Δ between the cells in the gHCO, in which each cell is an exponential IF-model (b).

for the desired gaits, the time-scale of the synapses in its circuitry should be swapped: slow inhibitory synapses with PSP summation and FTM-fast excitatory ones without PSP summation, see the Appendix for details. Moreover, we use a modified version of the first-order synapse to model slow inhibitory synapses. The dynamics of its activation is governed by the following equation

$$\frac{ds_i}{dt} = \alpha s_i (1 - s_i) f_\infty(V_i) - \beta s_i \quad (4)$$

where the new multiplicative term delays and hence slows down the synaptic activation for low spike-frequency in the pre-synaptic neuron; the synapse remains inactive near $I_c = -0.43$. The synapse given by Eq. 4 maintains a greater contrast in the mean s_i -values corresponding to the low and high ends of the bursting I_c -range for the given neuron model.

The results are summarized in Fig. 7, representing the bifurcation diagram for this gHCO. It demonstrates that the gHCO bursters oscillate robustly in-phase ($\Delta = \{0, 1\}$) for negative I_c -values and rapidly transition to the stable anti-phase ($\Delta = 0.5$), phase-locked state as the drive is increased above -0.2. Despite the abrupt jump in the bifurcation diagram, the time evolution between in-phase and anti-phase bursting occurs smoothly (see Fig. 8) as the control current I_c is step-wise increased from -0.43 to 0.13.

VI. CONCLUDING REMARKS

We developed a generalized HCO-model with a short-term plasticity mechanism, which accounts for short timescale gait transitions induced by sensory input or cognitive tasks. The proposed concept is based on simple constraints (i) subjecting models for cells and synapses and (ii) optimizing the trading-off between physiological plausibility and model functionality. The generality of our approach suggests that it will be applicable for other biologically plausible and phenomenological models of endogenous (square-wave) bursters, and for other dynamic synapse models.

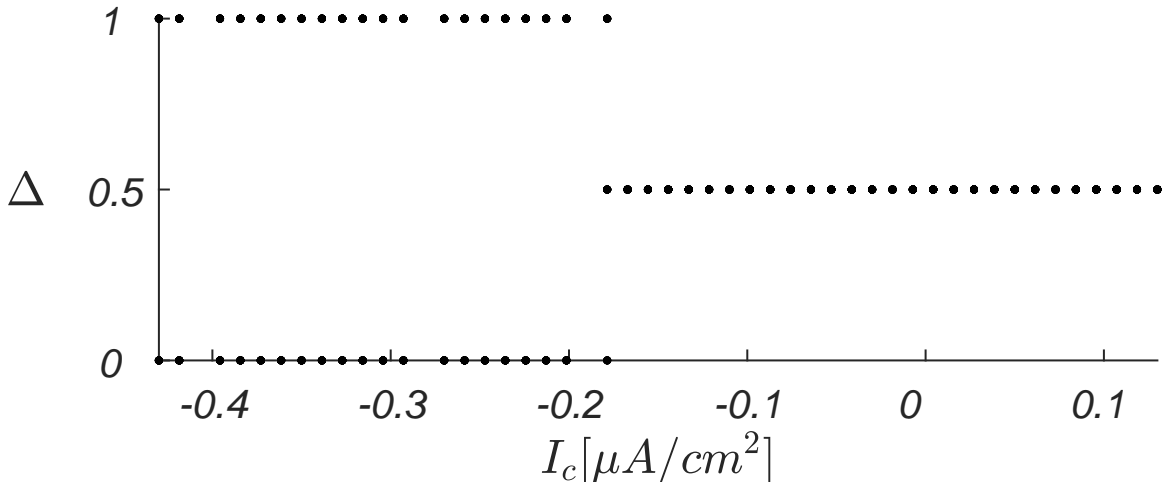


FIG. 7. Bifurcation diagram showing the flat-even phase-lags, $\Delta = \{0, 1\}$ (in-phase) and $\Delta = 0.5$ (anti-phase), between the bursters plotted against the current I_c for the gHCO with slow inhibitory and fast excitatory synapses; here, 30 initial Δ -values were sampled evenly between 0.05 and 0.95 for every I_c value out of 50. Parameters listed in the Appendix.

ACKNOWLEDGMENTS

We would like to acknowledge J. Scully's contribution to the concept and development of the synapse model Eq. (4). A.S.'s research was partially funded by the NSF grant IOS-1455527. M.S. and A.S. conceptualized the work; V.B. and M.L. conducted the experiments.

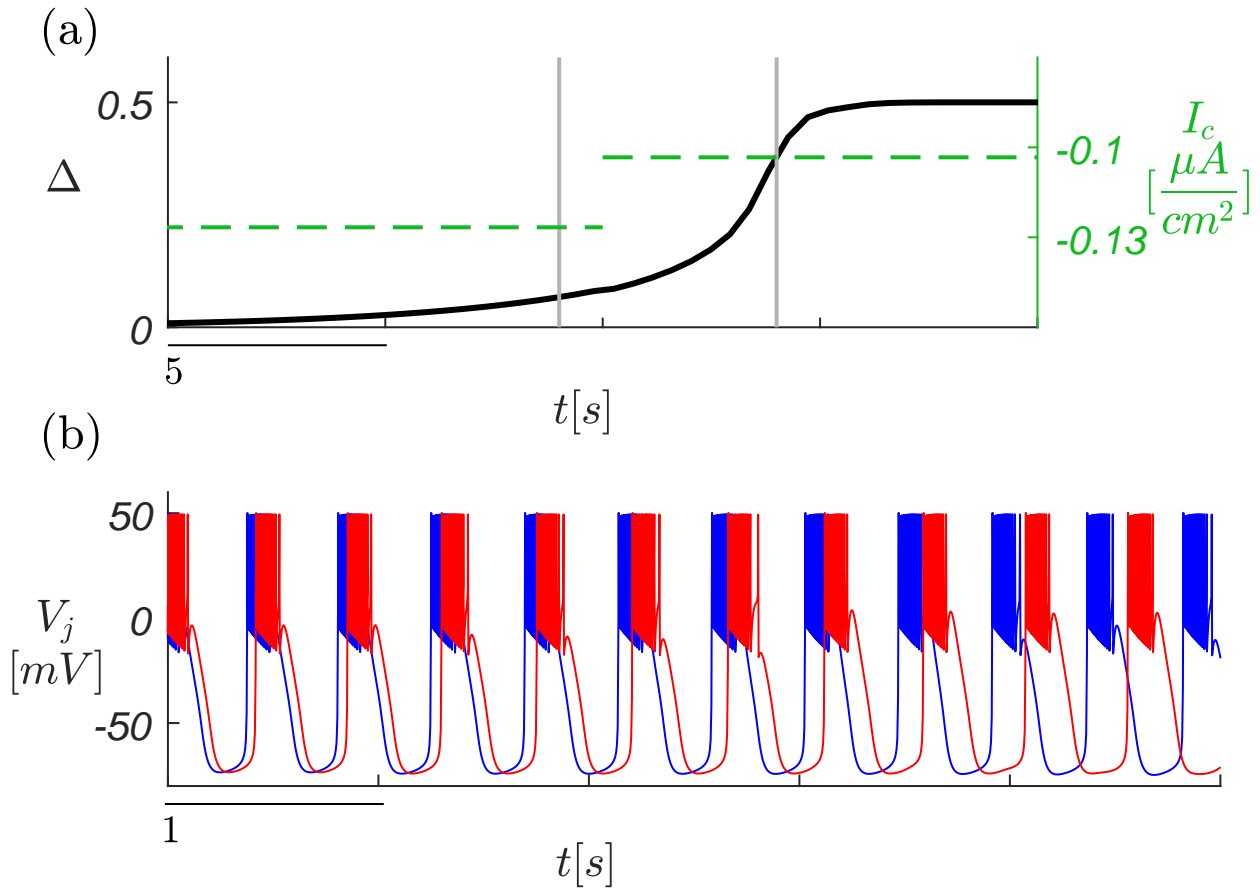


FIG. 8. (color online) (a) Time evolution of the phase lag Δ between the gHCO cells (black line) in response to step-wise changes of I_c (green dashed lines); I_c increased over 25 steps from -0.43 to 0.13 , only the time window in which Δ transition occurs is shown. (b) Voltage traces progressing from in-phase to anti-phase bursting within the time window bounded by the grey vertical lines in (a).

Appendix A: Neuron Models

1. Thalamic Reticular Neuron Model

The thalamic reticular neuron model [13, 28] is defined by the following state equations:

$$\begin{cases} \frac{dV}{dt} = \frac{-I_T - I_L - I_{Na} - I_K - I_c + I^{syn}}{C} \\ \frac{dCa}{dt} = -\frac{kI_T}{2Fd} - \frac{K_T Ca}{Ca + K_d} \\ \frac{dy}{dt} = \frac{y^\infty - y}{\tau_y} \quad y = \{h, m, n, m_T, h_T\} \end{cases} \quad (\text{A1})$$

where V is the membrane potential of the neuron; the ion currents I_T (calcium), I_{Na} (sodium), I_K (potassium), and I_L (leakage) evolve according to the following equations

$$\begin{aligned} I_T &= g_{Ca} m_T^2 h_T (V - E_{Ca}), & I_L &= g_L (V - E_L), \\ I_{Na} &= g_{Na} m^3 h (V - E_{Na}), & I_K &= g_k n^4 (V - E_k), \end{aligned}$$

which depend on V , on the intracellular calcium concentration Ca and on a set of further state variables (called *gating variables*) h, m, n, m_T, h_T . The differential equations governing these gating variables have the common structure written above (for the generic gating variable y), where:

$$\begin{aligned} y^\infty &= a_y / (a_y + b_y), & \tau_y &= 1 / (a_y + b_y) \quad (y = \{h, m, n\}) \\ a_h &= 0.128 e^{\frac{17-V}{18}}, & b_h &= \frac{4}{e^{-0.2(V-40)} + 1}, \\ a_m &= \frac{0.32(13-V)}{e^{0.25(13-V)} - 1}, & b_m &= \frac{0.28(V-40)}{e^{0.2(V-40)} - 1} \\ a_n &= \frac{0.032(15-V)}{e^{0.2(15-V)} - 1}, & b_n &= 0.5 e^{\frac{10-V}{40}} \\ m_T^\infty &= \frac{1}{1 + e^{-\frac{V+52}{7.4}}}, & \tau_{mT} &= 0.44 + \frac{0.15}{e^{\frac{V+27}{10}} + e^{-\frac{V+102}{15}}}, \\ h_T^\infty &= \frac{1}{1 + e^{\frac{V+80}{5}}}, & \tau_{hT} &= 62.7 + \frac{0.27}{e^{\frac{V+48}{4}} + e^{-\frac{V+407}{50}}}. \end{aligned}$$

In the above equations, h and m are the inactivation and activation variables of the Na^+ current; n is the activation variable of the K^+ current; m_T and h_T are the activation and inactivation variables of the low-threshold Ca^{2+} current; the leakage current I_L has conductance $g_L = 0.05 \frac{mS}{cm^2}$ and reversal potential $E_L = -78 [mV]$; I_{Na} and I_K are the

fast Na^+ and K^+ currents responsible for the generation of action potentials, with conductances $g_{Na} = 100 [\frac{mS}{cm^2}]$ and $g_k = 10 [\frac{mS}{cm^2}]$ and reversal potentials $E_{Na} = 50 [mV]$ and $E_k = -95 [mV]$; I_T is the low-threshold Ca^{2+} current that mediates the rebound burst response, with conductance $g_{Ca} = 1.75 [\frac{mS}{cm^2}]$ and reversal potential $E_{Ca} = k_0 \frac{RT}{2F} \log(\frac{Ca_0}{C_a})$; I^{syn} is the synaptic current (Eq. (2) in the paper).

When the control current I_c is in the range $[-0.43, 0.13] [\frac{\mu A}{cm^2}]$ the neuron exhibits bursting behavior. The other parameters are set as follows: $C = 1 [\frac{\mu F}{cm^2}]$, $Ca_0 = 2 [mM]$, $d = 1 [\mu m]$, $K_T = 0.0001 [mM \cdot ms]$, $K_d = 0.0001 [mM]$. $F = 96.489 [\frac{C}{mol}]$ is the Faraday constant, $R = 8.31441 [\frac{J}{mol \cdot K}]$ is the universal gas constant and the temperature T is set at $309.15 [K]$.

2. Exponential Integrate and Fire Neuron Model

The exponential integrate and fire (eIF) neuron model [5] is defined by the following state equations:

$$\begin{cases} \frac{dV}{dt} = \frac{-g_L(V - E_L) + g_e e^{\frac{V - V_T}{\Delta_T}} - u + I_{ext} + I^{syn}}{C} \\ \frac{du}{dt} = \frac{a(V - E_L) - u}{\tau_w} \end{cases} \quad (A2)$$

where V is the membrane potential of the neuron; u is the adaptation variable; $g_L = 30 [nS]$ is the leakage conductance and $E_L = -70.6 [mV]$ is the leakage reversal potential; I^{syn} is the synaptic current (Eq. (2) in the paper).

When the conductance g_e is set at $110 [nS]$, the external current I_{ext} is varied in the range $[690, 1110] [pA]$ (Fig. 5). When the external current I_{ext} is set at $800 [pA]$, the conductance g_e is varied in the range $[20, 160] [nS]$ (Fig. 6). For this range of parameter values, the neuron exhibits bursting behavior. The other parameters are set as follows: $C = 2007.4 [pF]$, $V_T = -50.4 [mV]$, $\Delta_T = 2 [mV]$, $\tau_w = 285.7 [ms]$, $a = 4 [nS]$.

3. Plant Neuron Model

The Plant neuron model [1, 31] is defined by the following state equations:

$$\left\{ \begin{array}{l} \frac{dV}{dt} = \frac{-I_T - I_L - I_{Na} - I_K - I_{KCa} + I_{ext} + I^{syn}}{C} \\ \frac{dCa}{dt} = \rho(K_c x (V_{Ca} - V) - Ca) \\ \frac{dy}{dt} = \frac{y^\infty - y}{\tau_y} \quad y = \{h, n, x\} \end{array} \right. \quad (A3)$$

where

$$I_T = g_T x (V - E_I), \quad I_L = g_L (V - E_L),$$

$$I_{Na} = g_I m_\infty^3 h (V - E_I), \quad I_K = g_K n^4 (V - E_K),$$

$$I_{KCa} = g_{KCa} \frac{Ca}{Ca + 0.5} (V - E_K),$$

$$m_\infty = \frac{\frac{0.1(50-V_s)}{e^{\frac{50-V_s}{10}}}}{\frac{0.1(50-V_s)}{e^{\frac{50-V_s}{10}}} + 4e^{\frac{25-V_s}{18}}},$$

$$h^\infty = \frac{0.07e^{\frac{25-V_s}{20}}}{0.07e^{\frac{25-V_s}{20}} + \frac{1}{1+e^{\frac{55-V_s}{10}}}},$$

$$\tau_h = \frac{12.5}{0.07e^{\frac{25-V_s}{20}} + \frac{1}{1+e^{\frac{55-V_s}{10}}}},$$

$$n^\infty = \frac{\frac{0.01(55-V_s)}{e^{\frac{55-V_s}{10}}} - 1}{\frac{0.01(55-V_s)}{e^{\frac{55-V_s}{10}}} - 1 + 0.125e^{\frac{45-V_s}{80}}},$$

$$\tau_n = \frac{12.5}{\frac{0.01(55-V_s)}{e^{\frac{55-V_s}{10}}} - 1 + 0.125e^{\frac{45-V_s}{80}}},$$

$$x^\infty = \frac{1}{e^{0.15(-V-50)} + 1},$$

$$V_s = \frac{127V}{105} + \frac{8265}{105}$$

where V is the membrane potential of the neuron; Ca is the intracellular calcium concentration; x is the activation variable of the slow inward Ca^{2+} current; h is the inactivation variable of the Na^+ current; n is the activation variable of the K^+ current; I_L is the leakage current, with conductance $g_L = 0.003 [nS]$ and reversal potential $E_L = -40 [mV]$; I_{Na} and I_K are the fast inward Na^+ and outward K^+ currents, respectively, with conductances $g_I = 8 [nS]$ and $g_K = 1.3 [nS]$ (these values ensure undershoot, see paper) and reversal potentials $E_I = 30mV$ and $E_K = -75 [mV]$; I_T is the slow inward tetrodotoxin-resistant

Ca^{2+} current, with conductance $g_T = 0.01 [nS]$ and reversal potential $E_T = 30 [mV]$; I_{KCa} is the outward Ca^{2+} sensitive K^+ current, with conductance $g_{KCa} = 0.03 [nS]$ and reversal potential E_K ; I^{syn} is the synaptic current (Eq. (2) in the paper).

The external current I_{ext} is set to $0.028 [\mu A]$. The other parameters are set as follows: $C = 1 [\frac{\mu F}{cm^2}]$, $\rho = 0.00015 [mV^{-1}]$, $K_c = 0.0085 [mV^{-1}]$, $V_{Ca} = 140 [mV]$, $\tau_x = 235 [ms]$.

Appendix B: Synapse Parameter Values

In Table I, column A lists the parameter values used for the gHCO with the thalamic reticular neuron model, first-order dynamic excitatory synapses and static inhibitory synapses (Figs. 2 and 3). Column B lists the parameter values used when simulating the gHCO with the thalamic reticular neuron model, modified first-order dynamic inhibitory synapses (Eq. 4) and static excitatory synapses (Figs. 7 and 8 in the paper). Column C lists the parameter values used for the gHCO with the eIF neuron model when varying I_{ext} , first-order dynamic excitatory synapses and static inhibitory synapses (Fig. 5). Column D lists the parameter values used for the gHCO with the eIF neuron model when varying g_e , first-order dynamic excitatory synapses and static inhibitory synapses (Fig. 6). Column E lists the parameter values used for the gHCO with the Plant neuron model, first-order dynamic excitatory synapses and static inhibitory synapses (Fig. 4).

-
- [1] Deniz Alaçam and Andrey Shilnikov. Making a swim central pattern generator out of latent parabolic bursters. *Int. J. Bifurcat. Chaos*, 25(07):1540003, 2015.
 - [2] Jessica Ausborn, Abigail C Snyder, Natalia A Shevtsova, Ilya A Rybak, and Jonathan E Rubin. State-dependent rhythmogenesis and frequency control in a half-center locomotor cpg. *J. Neurophysiol.*, 119(1):96–117, 2018.
 - [3] Carmelo Bellardita and Ole Kiehn. Phenotypic characterization of speed-associated gait changes in mice reveals modular organization of locomotor networks. *Curr. Biol.*, 25(11):1426–1436, 2015.
 - [4] Tiaza Bem and John Rinzel. Short duty cycle destabilizes a half-center oscillator, but gap junctions can restabilize the anti-phase pattern. *J. Neurophysiol.*, 91(2):693–703, 2004.

TABLE I. Parameter values.

	A	B	C	D	E
α^{ex}	0.1556	-	10	10	0.5
β^{ex}	0.005	-	0.26	26	0.0005
θ^{ex}	25	-30	-40	-40	-42
g^{ex}	0.0005	0.00001	1	0.4	0.0001
E^{ex}	60	60	20	20	50
α^{in}	-	0.5	-	-	-
β^{in}	-	0.02	-	-	-
θ^{in}	-30	25	-48.5	-48.5	-53
g^{in}	0.0005	0.01	0.6	0.1	0.0001
E^{in}	-80	-80	-110	-110	-80
ν	10	10	10	10	10

- [5] Romain Brette and Wulfram Gerstner. Adaptive exponential integrate-and-fire model as an effective description of neuronal activity. *J. Neurophysiol.*, 94(5):3637–3642, 2005.
- [6] T Graham Brown. On the nature of the fundamental activity of the nervous centres; together with an analysis of the conditioning of rhythmic activity in progression, and a theory of the evolution of function in the nervous system. *J. Physiol.*, 48(1):18–46, 1914.
- [7] Pietro-Luciano Buono and Martin Golubitsky. Models of central pattern generators for quadruped locomotion i. primary gaits. *J. Math. Biol.*, 42(4):291–326, 2001.
- [8] Dean V Buonomano. Decoding temporal information: a model based on short-term synaptic plasticity. *J. Neurosci.*, 20(3):1129–1141, 2000.
- [9] Vittorio Caggiano, Roberto Leiras, Haizea Goñi-Erro, Debora Masini, Carmelo Bellardita, Julien Bouvier, V Caldeira, Gilberto Fisone, and Ole Kiehn. Midbrain circuits that set locomotor speed and gait selection. *Nature*, 553(7689):455–460, 2018.
- [10] Ronald L Calabrese. Half-center oscillators underlying rhythmic movements. *Nature*, 261:146–148, 1995.
- [11] N Dale and A Roberts. Dual-component amino-acid-mediated synaptic potentials: excitatory drive for swimming in xenopus embryos. *J. Physiol.*, 363(1):35–59, 1985.

- [12] Simon M Danner, Natalia A Shevtsova, Alain Frigon, and Ilya A Rybak. Computational modeling of spinal circuits controlling limb coordination and gaits in quadrupeds. *Elife*, 6:e31050, 2017.
- [13] Alain Destexhe, Diego Contreras, Terrence J Sejnowski, and Mircea Steriade. A model of spindle rhythmicity in the isolated thalamic reticular nucleus. *J. Neurophysiol.*, 72(2):803–818, 1994.
- [14] Anca Doloc-Mihu and Ronald L Calabrese. A database of computational models of a half-center oscillator for analyzing how neuronal parameters influence network activity. *J. Biol. Phys.*, 37(3):263–283, 2011.
- [15] Sten Grillner. Biological pattern generation: the cellular and computational logic of networks in motion. *Neuron*, 52(5):751–766, 2006.
- [16] Charuni Gunaratne, Akira Sakurai, and Paul S. Katz. Variations on a theme: species differences in synaptic connectivity do not predict central pattern generator activity. *J. Neurophysiol.*, 118:1123–1132, 2017.
- [17] Ronald M. Harris-Warrick and Jan-Marino Ramirez. Neural networks for the generation of rhythmic motor behaviors. In *Neurobiology of Motor Control*, chapter 8, pages 225–262. 2017.
- [18] Auke Jan Ijspeert. Central pattern generators for locomotion control in animals and robots: a review. *Neur. Netw.*, 21(4):642–653, 2008.
- [19] Eugene M Izhikevich. Neural excitability, spiking and bursting. *Int. J. Bifurcat. Chaos*, 10(06):1171–1266, 2000.
- [20] Saijiya Jalil, Dane Allen, Joseph Youker, and Andrey Shilnikov. Toward robust phase-locking in melibe swim central pattern generator models. *Chaos*, 23(4):046105, 2013.
- [21] Saijiya Jalil, Igor Belykh, and Andrey Shilnikov. Spikes matter for phase-locked bursting in inhibitory neurons. *Phys. Rev. E*, 85(3):036214, 2012.
- [22] Ole Kiehn and Kimberly Dougherty. Locomotion: circuits and physiology. In *Neuroscience in the 21st Century*, pages 1337–1365. Springer, 2016.
- [23] Maxime Lemieux, Nicolas Josset, Marie Roussel, Sébastien Couraud, and Frédéric Bretzner. Speed-dependent modulation of the locomotor behavior in adult mice reveals attractor and transitional gaits. *Front. Neurosci.*, 10:42, 2016.
- [24] Matteo Lodi, Andrey Shilnikov, and Marco Storace. CEPAGEs: a toolbox for central pattern generator analysis. In *Proc. IEEE ISCAS*, pages 1–4, 2017.

- [25] Matteo Lodi, Andrey Shilnikov, and Marco Storace. Design of synthetic central pattern generators producing desired quadruped gaits. *IEEE Trans. Circ. Syst. I*, 65(3):1028–1039, 2017.
- [26] Matteo Lodi, Andrey L Shilnikov, and Marco Storace. Design principles for central pattern generators with preset rhythms. *IEEE Trans. Neural Netw. Learn. Syst.*, 2020.
- [27] Yaroslav I Molkov, Bartholomew J Bacak, Adolfo E Talpalar, and Ilya A Rybak. Mechanisms of left-right coordination in mammalian locomotor pattern generation circuits: a mathematical modeling view. *PLoS Comp. Biol.*, 11(5), 2015.
- [28] Roman Nagornov, Grigory Osipov, Maxim Komarov, Arkady Pikovsky, and Andrey Shilnikov. Mixed-mode synchronization between two inhibitory neurons with post-inhibitory rebound. *Commun. Nonlinear Sci.*, 36:175–191, 2016.
- [29] M Pinco and A Lev-Tov. Synaptic transmission between ventrolateral funiculus axons and lumbar motoneurons in the isolated spinal cord of the neonatal rat. *J. Neurophysiol.*, 72(5):2406–2419, 1994.
- [30] Carla MA Pinto and Martin Golubitsky. Central pattern generators for bipedal locomotion. *J. Math. Biol.*, 53(3):474–489, 2006.
- [31] Richard E Plant. Bifurcation and resonance in a model for bursting nerve cells. *J. Math. Biol.*, 11(1):15–32, 1981.
- [32] Akira Sakurai and Paul S. Katz. Command or obey? homologous neurons differ in hierarchical position for the generation of homologous behaviors. *J. Neurosci.*, 39(33):6460–6471, 2019.
- [33] David Somers and Nancy Kopell. Rapid synchronization through fast threshold modulation. *Biol. Cybern.*, 68(5):393–407, 1993.
- [34] Kaoru Takakusaki. Neurophysiology of gait: from the spinal cord to the frontal lobe. *Mov. Disord.*, 28(11):1483–1491, 2013.
- [35] X-J Wang. Fast burst firing and short-term synaptic plasticity: a model of neocortical chattering neurons. *Neurosci.*, 89(2):347–362, 1999.
- [36] Jeremy Wojcik, Justus Schwabedal, Robert Clewley, and Andrey L Shilnikov. Key bifurcations of bursting polyrhythms in 3-cell central pattern generators. *PloS One*, 9(4), 2014.
- [37] Junzhi Yu, Min Tan, Jian Chen, and Jianwei Zhang. A survey on cpg-inspired control models and system implementation. *IEEE Trans. Neural Netw. Learn. Syst.*, 25(3):441–456, 2013.

- [38] Le Zhao and Alain Nogaret. Experimental observation of multistability and dynamic attractors in silicon central pattern generators. *Phys. Rev. E*, 92(5):052910, 2015.